PNAS RESEARCH ARTICLE | IMMUNOLOGY AND INFLAMMATION

Mechanistic basis for potassium efflux–driven activation of the human NLRP1 inflammasome

Pritisha Rozario[a,1], Miriam Pinilla[b,1], Leana Gorse[b], Anna Constance Vind[c,d], Kim S. Robinson[e,f,2], Gee Ann Toh[a], Muhammad Jasrie Firdaus[a], José Francisco Martínez[c,d], Swat Kim Kerk[g], Zhewang Lin[h], John C. Chambers[g], Simon Bekker-Jensen[c,d], Etienne Meunier[b,3,4], and Franklin Zhong[a,f,3,4]

Edited by Hao Wu, Harvard Medical School, Boston, MA; received June 7, 2023; accepted November 15, 2023

Nigericin, an ionophore derived from *Streptomyces hygroscopicus*, is arguably the most commonly used tool compound to study the NLRP3 inflammasome. Recent findings, however, showed that nigericin also activates the NLRP1 inflammasome in human keratinocytes. In this study, we resolve the mechanistic basis of nigericin-driven NLRP1 inflammasome activation. In multiple nonhematopoietic cell types, nigericin rapidly and specifically inhibits the elongation stage of the ribosome cycle by depleting cytosolic potassium ions. This activates the ribotoxic stress response (RSR) sensor kinase ZAKα, p38, and JNK, as well as the hyperphosphorylation of the NLRP1 linker domain. As a result, nigericin-induced pyroptosis in human keratinocytes is blocked by extracellular potassium supplementation, ZAKα knockout, or pharmacologic inhibitors of ZAKα and p38 kinase activities. By surveying a panel of ionophores, we show that electroneutrality of ion movement is essential to activate ZAKα-driven RSR and a greater extent of K+ depletion is necessary to activate ZAKα-NLRP1 than NLRP3. These findings resolve the mechanism by which nigericin activates NLRP1 in nonhematopoietic cell types and demonstrate an unexpected connection between RSR, perturbations of potassium ion flux, and innate immunity.

innate immunity | inflammasome | NLRP1 | nigericin | potassium efflux

Significance

Nigericin is familiar to the inflammasome field as the commonly used NLRP3 inducer. It has enabled numerous breakthroughs in the field linking NLRP3 activation to potassium efflux. In this manuscript, we report that nigericin activates an alternate inflammasome sensor, NLRP1, in primary human skin, nasal, and corneal epithelial cells. NLRP1 activation by nigericin requires K+ efflux–driven ribosome stalling and the ribotoxic stress response (RSR) sensor MAP3K, ZAKα. We further identify the key biophysical principles that explain why only a subset of K+ ionophores, exemplified by nigericin, function as "super" inflammasome agonists that can activate either NLRP1 or NLRP3, depending on cell type. These results reveal an unexpected connection between RSR, potassium ion flux, and innate immunity.

It has been estimated that mammalian cells consume up to ~70% of the total energy expenditure actively transporting sodium and potassium ions across the plasma membrane, creating a high potassium (~140 mM) and low sodium (~5 to 15 mM) environment in the cytosol relative to the extracellular space (1). The resulting electrochemical potential across the plasma membrane is essential to many physiological processes, e.g., intracellular uptake of nutrients, transmission of neuronal action potential, and contraction of muscles among others. Dysregulation of resting-state membrane potential, as well as stimulus-induced ion flux, can cause a variety of human diseases, including neurological disorders, cystic fibrosis and heart failure (2, 3).

Ionophores are molecules that facilitate the transport of ions across lipid bilayers and are widely used as chemical probes to study the biological function of ionic flux or as pharmacologic agents to manipulate ionic homeostasis in vivo (4, 5). Nigericin (CAS 28643-80-3), a secondary metabolite isolated from *Streptomyces hygroscopicus*, is a well-studied carrier-type ionophore that specifically "antiports" potassium ions in exchange for protons. This process allows both ions to flow down their electrochemical gradients without incurring a net electrical charge (electroneutral) and is therefore thermodynamically favorable. As a result, nigericin is capable of completely dissipating the K+ and proton gradients where they run in opposite directions, e.g., across the plasma membrane of mammalian cells. Due to this property, nigericin has been widely used in chemistry as a K+ or proton "clamp" to ensure stable equalization of the respective ionic concentrations across diffusion barrier membranes or to probe the consequences of K+ movements in biological systems (6).

The plasma membrane of eukaryotic cells is prone to damage caused by environmental toxins, endogenous danger signals, and microbial infections, all of which can lead to the leakage of cytosolic K+ ions into the extracellular space. In vertebrate species, K+ efflux is specifically sensed by a conserved intracellular innate sensor protein known as NLRP3 (7–12). The depletion of cytosolic potassium ions below a certain concentration, which could be caused by ionophores, pore-forming toxins, and the opening of ion channels, causes NLRP3 to rapidly oligomerize and assemble the "inflammasome" complex, which in turn activates pro-caspase-1 via the adaptor protein ASC. This process induces rapid pyroptotic cell death via the pore-forming protein GSDMD and the secretion of pro-inflammatory cytokines in the IL-1 family. Due to its ability to rapidly trigger K+ efflux, nigericin is arguably the most widely used agonist to probe NLRP3 function. For

The authors declare no competing interest.

This article is a PNAS Direct Submission.

[1]P.R. and M.P. contributed equally to this work.

[2]Present address: Skin Research Centre, Department of Hull York Medical School, University of York, York Y010 5DD, United Kingdom.

[3]To whom correspondence may be addressed. Email: etienne.meunier@ipbs.fr or franklin.zhong@ntu.edu.sg.

[4]E.M. and F.Z. contributed equally to this work.

This article contains supporting information online at https://www.pnas.org/lookup/suppl/doi:10.1073/pnas.2309579121/-/DCSupplemental.

Published January 4, 2024.

instance, nigericin was instrumental in enabling the elucidation of the atomic structure of activated NLRP3 (11, 13–15). It was also used to uncover the critical involvement of trans-Golgi and vesicular lipid molecules in NLRP3 function (16–18). It is generally thought that nigericin is an exclusive NLRP3 agonist, at least in hematopoietic cell types, as numerous studies demonstrated that chemical inhibition or genetic ablation of NLRP3 completely abrogates nigericin-driven pyroptosis in human and murine macrophages and monocytes, while other inflammasome sensors, such as NLRC4, AIM2, and MEFV (9, 19), do not respond to nigericin. As such, nigericin-driven pyroptosis is often used as a diagnostic test for NLRP3 functionality in various experimental systems.

Notwithstanding the indisputable evidence showing that nigericin activates NLRP3, some studies suggest that nigericin has NLRP3-independent functions in programmed cell death. For instance, nigericin is cytotoxic in many human cancer cell lines with IC50 ~5 μM, including those that do not express inflammasome components (20). Recent studies additionally demonstrated that nigericin can induce pyroptosis in human keratinocytes via another inflammasome sensor protein known as NLRP1 (21, 22), which is predominantly expressed in human skin and airway and does not share the same agonist repertoire as NLRP3 (23, 24). These findings prompted us to reexamine the role of nigericin outside the context of NLRP3 agonism. Here, we report that nigericin-induced K+ efflux inhibits protein synthesis due to a specific block of the ribosomal elongation cycle. By doing so, nigericin functions as a potent inducer of the ZAKα-dependent ribotoxic stress response (RSR) in numerous human cell lines, and NLRP1 activator more specifically in primary human epithelial cells. By characterizing a range of ionophores, we find that RSR/NLRP1 induction requires electroneutrality of K+ efflux and >20% of K+ depletion from the intracellular store. This explains why only K+/H+ antiporters, exemplified by nigericin and the veterinary antibiotic lasalocid acid (8, 25), are capable of activating both NLRP1 and NLRP3. Our results shed light on how nigericin activates the NLRP1 inflammasome in nonhematopoietic cell types and suggest that RSR and the NLRP1 inflammasome have a conserved function in the innate immune defense against perturbations of ionic potential.

Results

Nigericin-Driven Pyroptosis in Human Epithelial Cells Depends on NLRP1 and Potassium Efflux. We first sought to validate the findings by Fenini et al demonstrating that nigericin activates NLRP1 (21). In independently generated primary keratinocytes derived from healthy donors, nigericin indeed caused cardinal features of pyroptosis in a dose-dependent manner, as evidenced by membrane swelling (Fig. 1*A*), GSDMD cleavage (Fig. 1*B*), ASC speck formation (Fig. 1*C* and *SI Appendix*, Fig. S1*F*), rapid propidium iodide (PI) uptake within 3 h (*SI Appendix*, Fig. S1 *A* and *B*), and IL-1 secretion (Fig. 1*B* and *SI Appendix*, Fig. S1*C*). Using IL-1β secretion as a readout, the EC50 of nigericin is estimated to be 1.38 ± 0.28 μM (*SI Appendix*, Fig. S1*C*), which is similar to the concentrations commonly used to activate NLRP3 in macrophages. Importantly, nigericin-driven inflammasome assembly and pyroptosis are abrogated by caspase-1 inhibitor belnacasan (*SI Appendix*, Fig. S1*E*) or CRISPR/Cas9 KO of *NLRP1* in primary keratinocytes (Fig. 1 *E* and *F* and *SI Appendix*, Fig. S2*C*), but is insensitive to the NLRP3 inhibitor MCC950 (*SI Appendix*, Fig. S2 *A* and *B*). This is in contrast to macrophage-like cell lines, THP1 or U937 where nigericin-triggered IL-1β secretion is completely abrogated by MCC950 (*SI Appendix*, Fig. S3 *A* and *B*). In fact, NLRP3 expression is undetectable by RNAseq in primary keratinocytes, while NLRP1 transcript is highly abundant, approaching levels of known keratinocyte markers such as keratin-1 (KRT1) (Fig. 1*D*). Incidentally, primary keratinocytes also do not express the P2RX7 receptor, which is an upstream regulator of NLRP3 in other cell types (Fig. 1*D*). Indeed, the P2RX7 ligand ATP also fails to activate pyroptosis in keratinocytes up to 10 mM (*SI Appendix*, Fig. S1*D*). Nigericin is also able to induce IL-18 secretion in primary human nasal epithelial cells (HNECs) and corneal epithelial cells (HCEs) in a NLRP1-dependent manner (Fig. 1*G* and *SI Appendix*, Fig. S2*D*) and ASC-GFP speck formation in a A549-NLRP1-ASC-GFP reporter cell line where NLRP1 is exogenously expressed (*SI Appendix*, Fig. S2 *E* and *F*). These results confirm that nigericin activates both endogenous and reconstituted NLRP1 inflammasome in epithelial cells. Curiously, we found that the immortalized keratinocyte cell line N/TERT-1 (also referred as N/TERT), which is commonly used to study the NLRP1 inflammasome, is relatively insensitive to nigericin (*SI Appendix*, Fig. S3*C*). These results are consistent with recent findings that N/TERT cells have reduced sensitivity to other NLRP1 agonists, especially bacterial ribotoxins such as DT and exoA (26), as compared to primary keratinocytes. Similar to DT, TNFα priming boosts nigericin-induced pyroptosis in N/TERT cells (*SI Appendix*, Fig. S3*D*). While the exact cause(s) remain unclear, it is worth noting that NLRP1 is repressed in most squamous carcinoma cell lines (which are of keratinocyte origin) (27). Thus, it is likely that the initial immortalization process which gave rise to N/TERT cells had been selected for lower NLRP1 expression and/or functionality (28). Regardless, this finding underscores the importance of using primary cells to investigate NLRP1 function in vitro. In all subsequent experiments, the effect of nigericin on pyroptosis was studied exclusively in primary cells, while N/TERT cells were used to study the upstream molecular mechanisms.

Next, we tested whether nigericin-dependent NLRP1 activation depends on K+ efflux. By directly quantifying intracellular K+ content, we found that nigericin induces a rapid loss of intracellular K+ content in primary keratinocytes within 5 min of treatment (Fig. 2*A*) and within 15 min in A549 cells (*SI Appendix*, Fig. S4*E*). Raising K+ concentration by 50 mM in the keratinocyte culture media (from 1.7 to 51.7 mM) prevents this loss (Fig. 2*B*). Extracellular KCl inhibited nigericin-induced IL-1β secretion (Fig. 2*C*), PI uptake (Fig. 2*D*), and GSDMD cleavage (*SI Appendix*, Fig. S4*C*) in a dose-dependent manner in primary keratinocytes, with an apparent IC50 of 7.2 mM (Fig. 2*C*) based on IL-1β ELISA. Although 50 mM KCl also had a mild inhibitory effect on VbP- and ANS-driven IL-1β secretion, this could be mostly accounted for by reduced levels of uncleaved pro-IL-1β (*SI Appendix*, Fig. S4*C*). The kinetics and extent of PI uptake following anisomycin (ANS) treatment is not affected by extracellular KCl (*SI Appendix*, Fig. S4 *A* and *B*). In addition, neither extracellular NaCl nor Ca^{2+} chelator BAPTA-AM significantly reduces IL-1β secretion caused by nigericin (Fig. 2*C* and *SI Appendix*, Fig. S4*D*). These data support the notion that similar to NLRP3, nigericin activates the NLRP1 inflammasome specifically via K+ efflux.

Nigericin Blocks Protein Synthesis and Induces Ribotoxic Stress (RSR) via Potassium Efflux. Even though NLRP3 and NLRP1 are generally not expressed in the same cell types (11, 17), it is conceptually conceivable that potassium efflux activates both sensors via the same mechanism. However, unlike NLRP3, activated NLRP1 localizes almost exclusively to ASC specks and not to any obvious organellar or endosomal structures (Fig. 1*C*). Recently, we and others reported that NLRP1 can be activated

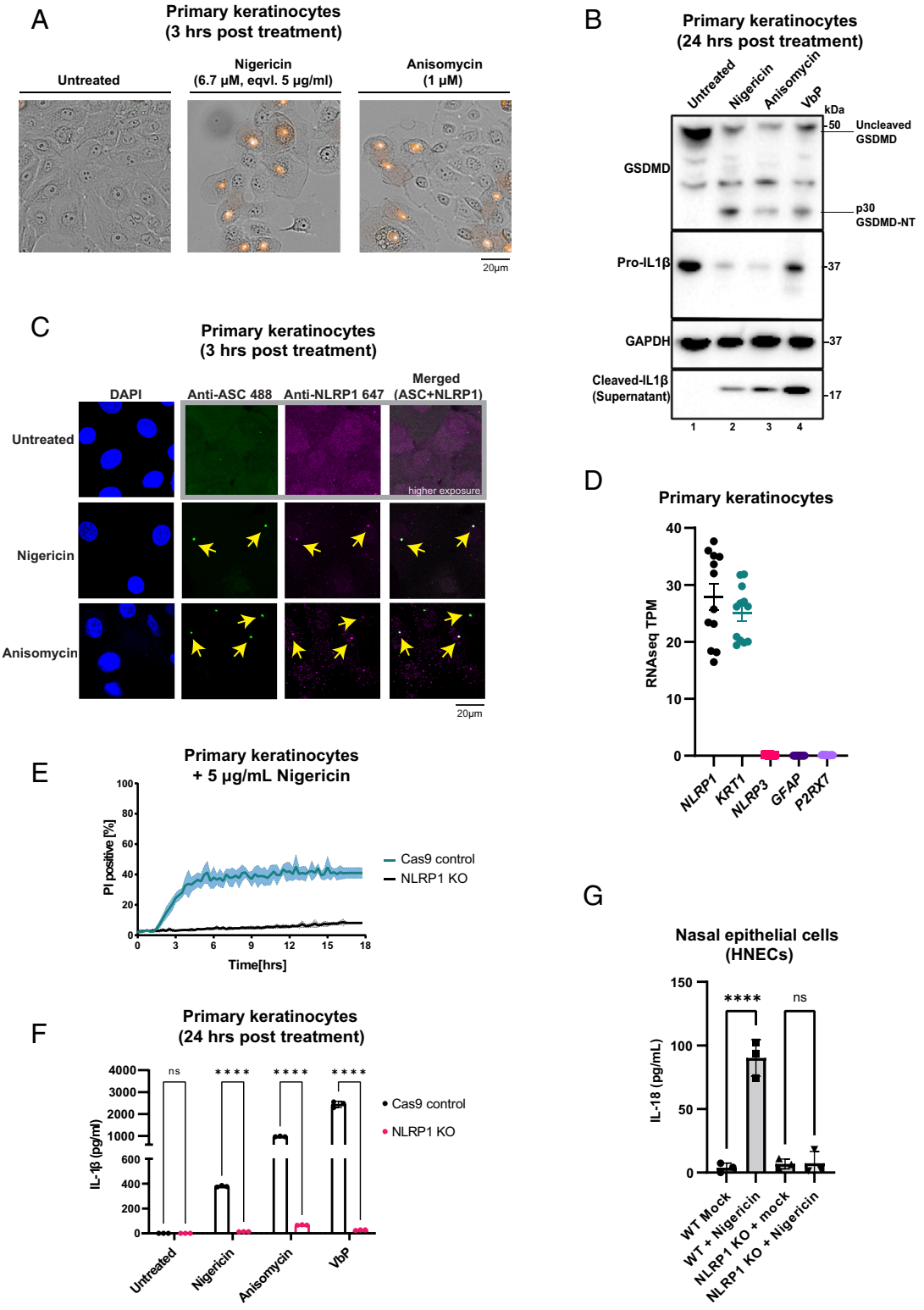

Fig. 1. (*A*) Representative bright-field microscopy images of primary keratinocytes showing propidium iodide (PI) inclusion 3 h posttreatment with nigericin (6.7 µM, equv. 5 µg/mL) or anisomycin (1 µM). Images are shown from one experiment and are representative of n = 3 independent experiments; scale bar, 20 µm. (*B*) Immublots of GSDMD (full length and cleaved), pro-IL1β, cleaved IL1β and GAPDH (loading control) in primary keratinocytes following overnight treatment with nigericin (5 µg/mL), anisomycin (1 µM) or VbP (3 µM). Immunoblot shows lysates from one experiment performed three independent times. (*C*) Representative confocal microscopy images showing ASC, NLRP1, and DAPI staining in primary keratinocytes pretreated with emricasan (5 µM) and stimulated with nigericin (5 µg/mL) or anisomycin (1 µM) for 3 h. Yellow arrows indicate speck formation by ASC and NLRP1. Images are shown from one experiment and are representative of n = 3 independent experiments; scale bar, 20 µm. (*D*) RNA-seq dataset of unstimulated primary keratinocytes (n = 9). TPM for a list of genes was plotted. (*E*) Quantification of the percentage of PI incorporation in Cas9 and NLRP1 KO primary keratinocytes upon nigericin (5 µg/mL) treatment. Cells were imaged at 15-min intervals for 18 h. (*F*) ELISA showing IL-1β secretion in Cas9 control and NLRP1 KO primary keratinocytes after nigericin (5 µg/mL), anisomycin (1 µM), or VbP (3 µM) treatment. Supernatant was harvested 24 h posttreatment. (*G*) ELISA showing IL-18 secretion in WT and NLRP1 KO primary HNECs after treatment with nigericin (5 µM). Supernatant was harvested 24 h posttreatment. Error bars represent SEM from three biological replicates, where one replicate refers to independent seeding and treatment of cells. Significance values were calculated based on two-way ANOVA followed by Sidak's test for multiple pairwise comparisons (*F* and *G*). ns, nonsignificant; **** $P < 0.0001$.

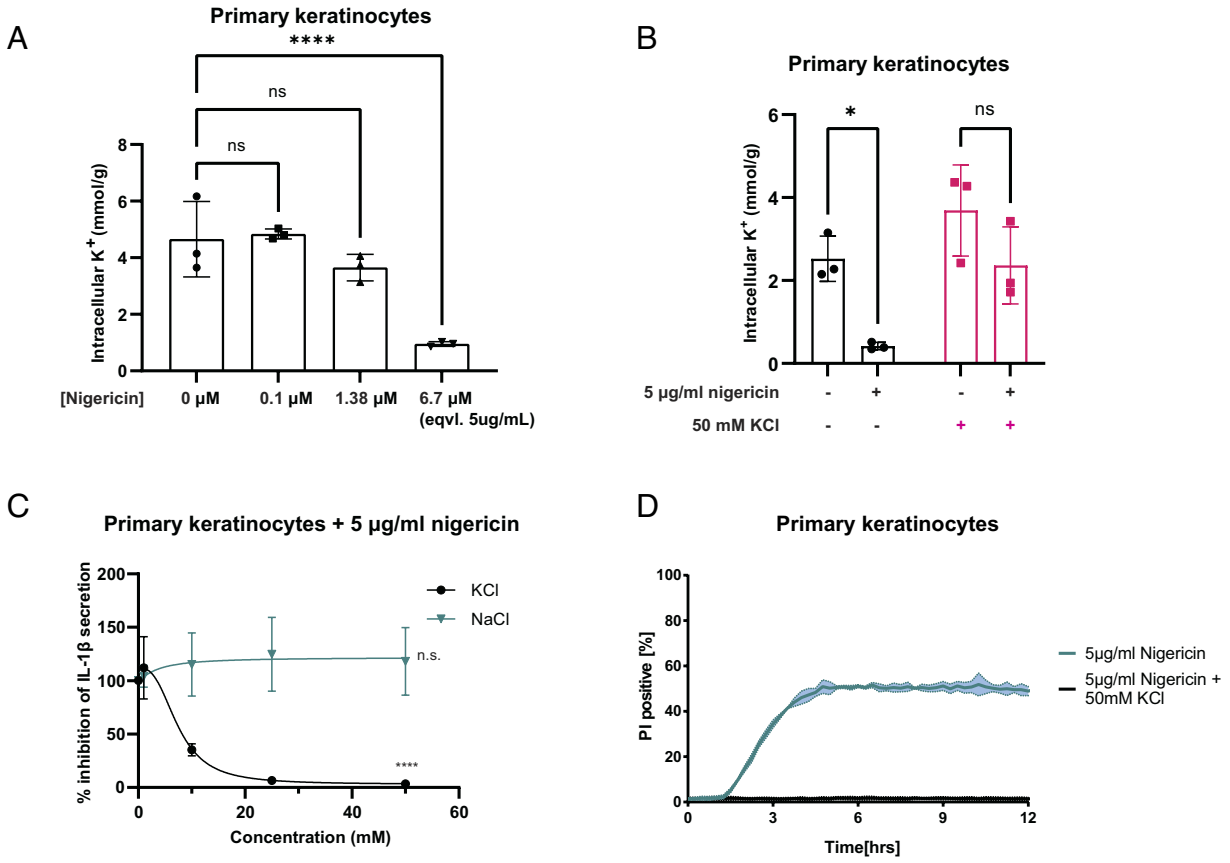

Fig. 2. (*A*) Quantification of intracellular K+ content by direct potentiometry in primary keratinocytes. Cells were pretreated with emricasan (5 µM) and then stimulated with nigericin (0.1 µM, 1.38 µM, or 6.7 µM) for 5 min. (*B*) In primary keratinocytes supplemented with 50 mM KCl 5 min prior to treatment with nigericin (5 µg/mL). (*C*) IL-1β ELISA showing the dose-dependent inhibitory response of KCl (IC50 = ~ 7.2 mM) and NaCl (IC50 = N.A.) in primary keratinocytes treated with nigericin (5 µg/mL). Supernatant was harvested 24 h posttreatment. (*D*) Quantification of the percentage of PI incorporation in primary keratinocytes supplemented with 50 mM KCl followed by nigericin (5 µg/mL) treatment. Cells were imaged at 15-min intervals for 18 h. Error bars represent SEM from three biological replicates, where one replicate refers to independent seeding and treatment of cells. Significance values were calculated based on one-way ANOVA followed by Dunnett's test (*A*) or two-way ANOVA followed by Sidak's test for multiple pairwise comparisons (*B* and *C*). ns, nonsignificant; *$P < 0.05$; ****$P < 0.0001$.

by the ribotoxic stress response kinase ZAKα downstream of ribosome stalling and/or collisions (26, 29–31). To the best of our knowledge, nigericin has not been linked to RSR, but several lines of evidence support this connection. First, nigericin and other NLRP3 agonists have been shown to inhibit protein synthesis in murine bone marrow–derived macrophages (32). In addition, in erythroid cell lysates in vitro, the rates of peptidyl transfer reaction by the ribosome are sensitive to potassium ion concentration (33). More importantly, updated atomic structures of the human ribosome complex revealed an abundance of potassium ions near the peptidyl transfer center (34). Based on these results, we hypothesized that nigericin activates NLRP1 via ZAKα-driven RSR. Indeed, 3 h of nigericin treatment led to a near complete cessation of de novo protein synthesis in primary keratinocytes, as revealed by the extent of puromycin incorporated into the nascent polypeptides (Fig. 3*A*, see *SI Appendix*, Fig. S5*A* for experimental setup). In addition, the effect of nigericin on translation requires the integrity of the plasma membrane, as the translation of a synthetic mRNA in rabbit reticulocyte lysates (RRL) is not inhibited, and even slightly enhanced, by nigericin (Fig. 3*B*). Furthermore, extracellular K+ at 50 mM restored protein synthesis in nigericin-treated cells (Fig. 3*C*, lane 5 vs. lane 8). These data suggest that nigericin inhibits translation indirectly by depleting K+ from the cytosol, rather than acting as a direct competitive/allosteric inhibitor of the ribosome.

To investigate which stage of the ribosome cycle is inhibited by K+ efflux, we carried out a harringtonine runoff assay in N/TERT cells (see *SI Appendix*, Fig. S5*B* for brief description of experimental setup), where the amount of puromycin-labeled nascent peptides is measured at regular intervals after the translational inhibition is blocked by harringtonine. In this assay, the time-dependent decrease in puromycin incorporation, i.e., the "runoff" rate, is directly proportional to the speed of ribosome elongation (35). In mock-treated cells, most of the ribosomes completed the runoff within 5 min. By contrast, in nigericin-treated cells, the level of puromycin-labeled proteins (albeit overall lower) remained unchanged across time, suggesting that the majority of the 80S ribosomes became arrested and were hence unable to incorporate puromycin into the nascent polypeptides (Fig. 3*C*). Importantly, supplementing culture media with 50 mM KCl restored the ribosome elongation to levels that are similar to untreated controls (Fig. 3*C*). Thus K+ efflux blocks the elongation stage of the ribosome cycle, resulting in ribosome stalling. It is critical to note that all aforementioned puromycin-incorporation assays (Fig. 3 *A* and *C*) were carried out in the presence of the pan-caspase inhibitor, emricasan, which blocks cell death including caspase-1-driven pyroptosis. Therefore, nigericin-driven ribotoxic stress occurs upstream, rather than downstream of cell death.

We next tested the effect of nigericin on U2OS cells, which do not express any inflammasome components but retain a fully functional RSR pathway (36, 37). Nigericin also causes ribosome stalling in a dose-dependent manner in U2OS cells, as evident in the increased amounts of polysomes at the expense of monosomes in the polysome gradient (Fig. 3 *D*, *Left*). In addition, by digesting lysates from nigericin-treated cells with MNase before resolving the polysomes on

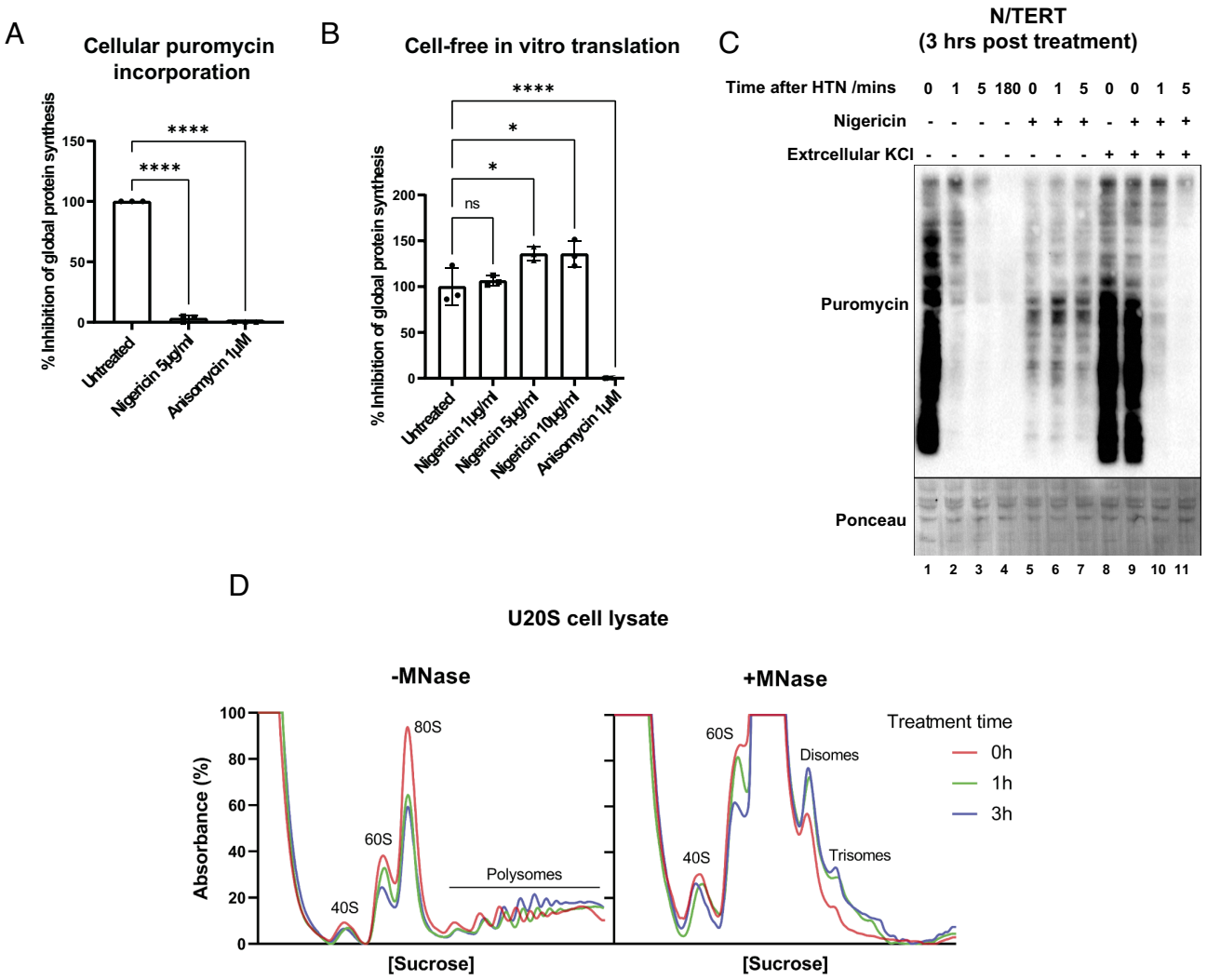

Fig. 3. (*A*) Quantification of the percentage inhibition of global protein synthesis in the cellular system (N/TERTs) following pretreatment with emricasan (5 μM) and 3-h treatment with nigericin (5 μg/mL) or anisomycin (1 μM). Protein synthesis was measured by normalized lane intensity in anti-puromycin blots performed three independent times. The percentage was calculated relative to untreated cells. (*B*) Quantification of the percentage inhibition of in vitro protein synthesis in the cell-free system (rabbit reticulocyte lysate) following 1-h treatment with nigericin (1 μg/mL, 5 μg/mL, or 10 μg/mL) or anisomycin (1 μM). Protein synthesis was measured by luciferase activity from three independent runs. The percentage was calculated relative to untreated lysate. (*C*) Immunoblotting of puromycin in N/TERTs following a ribosome runoff assay. Cells were pretreated with emricasan (5 μM) and stimulated with nigericin (5 μg/mL), ±KCl (50 mM) for 3 h before the addition of harringtonine (2 μg/mL) for the respective durations. Runoff was terminated by puromycin (10 μg/mL) for 10 min. Ponceau staining was used as the loading control. Immunoblot shows lysates from one experiment performed three independent times. (*D*) Sucrose gradient fractionation of undigested (*Left*) or MNase-digested (*Right*) U20S cell lysates following treatment with nigericin (10 μg/mL) for 1 h (green) or 3 h (blue). Error bars represent SEM from three biological replicates, where one replicate refers to independent seeding and treatment of cells. Significance values were calculated based on one-way ANOVA followed by Dunnett's test (*B* and *C*). ns, nonsignificant; *$P < 0.05$; ****$P < 0.0001$.

a sucrose gradient, we could detect the formation of "disomes" (Fig. 3 *D*, *Right*), which are MNase-resistant polysomes peaks indicating the presence of collided ribosomes. This was verified by orthogonal ribosome collection assays, such as the appearance of EDF1 in the ribosome pellet and RPS10 ubiquitination (*SI Appendix*, Fig. S5*C*). Thus, nigericin causes translational arrest by stalling elongating ribosomes in multiple cell types. Although it cannot be ruled out that nigericin affects other aspects of translation such as ribosome assembly, these effects were not apparent in the polysome gradient analysis, as the 80S peaks were still clearly present in nigericin-treated cells (Fig. 3 *D*, *Left*). Thus, nigericin-induced K+ efflux preferentially inhibits the elongation stage of the ribosome cycle, as predicted by previous in vitro and structural studies (33, 34).

ZAKα Is Required for Nigericin-Driven Pyroptosis in Nonhematopoietic Cells. We and others previously characterized the biochemical pathway by which a ribosome-bound kinase, ZAKα activates ribotoxic stress signaling in response to ribosome stalling/collisions (36–39). For unknown reasons, ribosome elongation inhibitors differ markedly in their abilities to activate ZAKα in a manner that is not correlated with their abilities to block protein synthesis. For instance, emetine and cycloheximide, are poor activators of ZAKα despite being strong inhibitors of global protein synthesis; whereas ANS and hygromycin act as strong activators of ZAKα (36, 37). In primary keratinocytes, we found that nigericin belongs to the latter group, as it strongly induces ZAKα autophosphorylation (Fig. 4*A*) and MAP2K-driven p38 and JNK phosphorylation in a K+ efflux–dependent manner (Fig. 4 *A* and *B*, lanes 4 to 6 vs. 7 to 9). Using a live cell imaging–based p38 and JNK Kinase Translocation Reporter (KTR) system (40, 41), we found that nigericin-induced JNK and p38 activation occurs at around 8 min after drug addition (Fig. 4 *C* and *D* and *SI Appendix*, Fig. S6 *A* and *B*) and is not noticeable before 5 min. Since K+ efflux within the first 5 min after nigericin treatment

(Fig. 2*A*), these results establish that K+ efflux occurs strictly prior to RSR induction. ZAKα KO abrogated nigericin as well as ANS-induced p38- and JNK-KTR translocation (Fig. 4*D* and *SI Appendix*, Fig. S6 *A* and *B*) and similarly eliminated JNK and p38 phosphorylation in nigericin-treated U2OS and HeLa cells (*SI Appendix*, Fig. S7 *A* and *B*). These findings corroborate that nigericin triggers bona fide ZAKα-driven RSR in a K+ efflux–dependent manner in a variety of cell types, including those that do not express NLRP1.

Next, we sought to distinguish whether K+ efflux-driven NLRP1 activation is due to the RSR MAPK signaling cascade or caused by some other signaling events initiated by stalled ribosomes. In the first test, we took advantage of the fact that a high dose of certain ribosome elongation inhibitors has an inverse dose response with regard to RSR induction, i.e., a high dose can block ribosome elongation without activating RSR (37). This is exemplified by the effect of emetine in primary keratinocytes. Emetine itself causes RSR at 10 μM, but not at 50 μM, as assayed by p38 and JNK phosphorylation (*SI Appendix*, Fig. S8 *A* and *B*). Pretreating primary keratinocytes with 50 μM emetine blocked nigericin- and ANS- induced ZAKα autophosphorylation and SAPK (p38/JNK) phosphorylation (*SI Appendix*, Fig. S8 *A* and *B*). Fifty micromolar emetine also abrogated nigericin-induced IL-1β secretion (*SI Appendix*, Fig. S8*C*). This epistatic analysis suggests that it is not ribosome stalling per se, but rather the induction of RSR that serves as the upstream signal for nigericin-driven (as well as ANS-driven) RSR in primary keratinocytes.

In the second test, we generated ZAKα KO primary keratinocytes and A549-ASC-GFP-NLRP1 reporter cells. In contrast to wild-type controls, nigericin did not induce IL-1β secretion or rapid PI uptake in ZAKα KO keratinocytes (Fig. 4*E* and *SI Appendix*, Fig. S9*A*) or ASC-GFP speck formation in ZAKα KO A549-ASC-GFP-NLRP1 cells (*SI Appendix*, Fig. S10 *A* and *B*). In addition, nigericin-driven NLRP1 activation can be inhibited by the same inhibitors as ANS-driven NLRP1 activation, including ZAKα inhibitors M443, compound 6p and p38 inhibitor Neflamapimod (*SI Appendix*, Fig. S9 *B* and *C*). In contrast, ZAKα inhibition did not affect nigericin-dependent NLRP3 activation in THP1 cells, which is completely inhibited by MCC950 (*SI Appendix*, Fig. S11 *A* and *B*). We have previously identified two putative ZAKα- and p38- substrate motifs (a.a. 112-114 and a.a. 1178-180) within the NLRP1 linker region, each consisting of three adjacent serines or threonine residues (29). NLRP1 mutants bearing phosph-dead mutations (serine/threonine to alanine) in these two motifs are significantly compromised in nigericin-induced activation, when overexpressed in NLRP1 KO N/TERT cells (*SI Appendix*, Fig. S9*D*) and a HEK293T-NLRP1-ASC-GFP reporter cell line (*SI Appendix*, Fig. S9 *E* and *F*). Although other phospho-residues probably also contribute to NLRP1 activation, these results show that nigericin activates NLRP1 exclusively through ZAKα-mediated phosphorylation in human epithelial cells.

Only Electroneutral, K+ Selective Ionophores, Exemplified by Nigericin and Lasalocid Acid, Activate NLRP1. Aside from nigericin, many molecules are known to activate NLRP3 by directly or indirectly inducing K+ efflux from the cytosol. We thus investigated whether ZAKα and NLRP1 can also be triggered by such a wide range of K+ efflux agents. To this end, we screened a panel of naturally occurring or synthetic ionophores or molecules with ionophore-like activities, including many that have previously been shown to activate NLRP3 (8, 9, 11) (Table 1). All compounds were screened as equivalent concentrations up to 10 μM. Their cellular effects on RSR and NLRP1 fell into three broad categories, which turned out to match precisely with their mechanisms of ion transport. Category I, exemplified by nigericin and lasalocid acid (a veterinary antibiotic), are electroneutral ionophores that selectively "antiport" K+ and H+, i.e., without causing charge separation across the plasma membrane. These molecules are known for their ability to equilibrate K+ and H+ gradients when they run in opposite directions, e.g., across the plasma membrane of mammalian cells. Both nigericin and lasalocid acid can induce full-blown RSR induction marked by ZAKα phosphorylation and SAPK activation (Fig. 5*A*) as a result of translational arrest and ribosome stalling (Fig. 5 *C* and *F*) Similar to nigericin, lasalocid causes inflammasome-driven pyroptosis in primary keratinocytes (Fig. 5 *B* and *D* and *SI Appendix*, Fig. S14*A*). NLRP1 KO or ZAKα chemical inhibition by M443 completely abrogated lasalocid acid–induced pyroptosis in primary keratinocytes (*SI Appendix*, Fig. S14 *B–E*). ZAKα KO also significantly, albeit partially, inhibited p38/JNK phosphorylation and p38/JNK KTR translocation triggered by lasalocid acid (*SI Appendix*, Figs. S12*B* and S13 *C* and *D*), suggesting that it can induce some ZAKα-independent stress signaling. In support of this notion, lasalocid was found to induce GSDME cleavage in an ZAKα-independent manner (*SI Appendix*, Fig. S14*B*, lanes 11 and 12).

Category II molecules consist of ionophores that transport K+ and/or other cations in an electrogenic fashion without the antiport of a cation or the "synport" of an anion (Table 1). Although they can permeabilize the plasma membrane toward K+, Nernst Law dictates that their ability to efflux K+ out of the cell must be limited by the concomitant creation of extra charge. This was confirmed via potentiometric titration with the most specific electrogenic K+ ionophore, valinomycin, which failed to cause a significant decrease in intracellular content in keratinocytes (Fig. 5*E*) up to 50 μM. We could not rule out the possibility that valinomycin could cause a small (<10%) reduction in intracellular K+ content, as the sensitivity of our initial potentiometry assay was approximately 0.5 mmol/g (normalized to total protein weight). Using a more sensitive method of K+ determination known as flame photometry, we found that higher concentration valinomycin (>7 μM) could indeed cause a small drop in intracellular K+ in A549-NLRP1-ASC-GFP cells, but it was ~10 times less effective than nigericin, with 10 μM valinomycin resulting in similar levels of reduction as 1 μM nigericin (*SI Appendix*, Fig. S13*A*). In primary keratinocytes, none of the category II ionophores had an obvious effect on protein synthesis and ribosome elongation (Fig. 5*C* and *SI Appendix*, Fig. S12*A*), or ZAKα/SAPK phosphorylation (Fig. 5*A*). Although cytotoxic, none of the category II ionophores including valinomycin caused IL-1β p17 secretion (Fig. 5 *B* and *D*) or GSDMD cleavage (*SI Appendix*, Fig. S12*E*) in primary keratinocytes. Despite ~20% reduction in intracellular K+ at concentrations >10 μM (*SI Appendix*, Fig. S13*A*), valinomycin failed to cause any ASC-GFP specks up to 20 μM in A549-ASC-GFP-NLRP1 cells (*SI Appendix*, Fig. S13*B*), demonstrating that this level of K+ efflux was insufficient to trigger RSR or the NLRP1 inflammasome. The overall lack of NLRP1 activation by valinomycin in multiple cell types stands in contrast to its known ability to activate NLRP3 in macrophages (11, 44). Our results thus suggest that ZAKα/NLRP1 is less sensitive to K+ efflux than NLRP3, and thus, a greater degree of K+ efflux is required to activate NLRP1 in epithelial cells (e.g., greater than 20% in A549 cells) than NLRP3 in macrophages.

The behaviors of category III molecules, gramicidin and palytoxin, shed further light on the relationship between K+ efflux, RSR and cell death. Gramicidin forms oligomeric channels in the plasma membrane that are permeable to many cations (45). Palytoxin is a marine toxin that locks the Na+/K+ ATPase pump into the open state, essentially converting it into a cation channel (46, 47). Despite their different modes of action, both molecules induce rapid outflow of K+ and inflow of Na+ and thus the complete

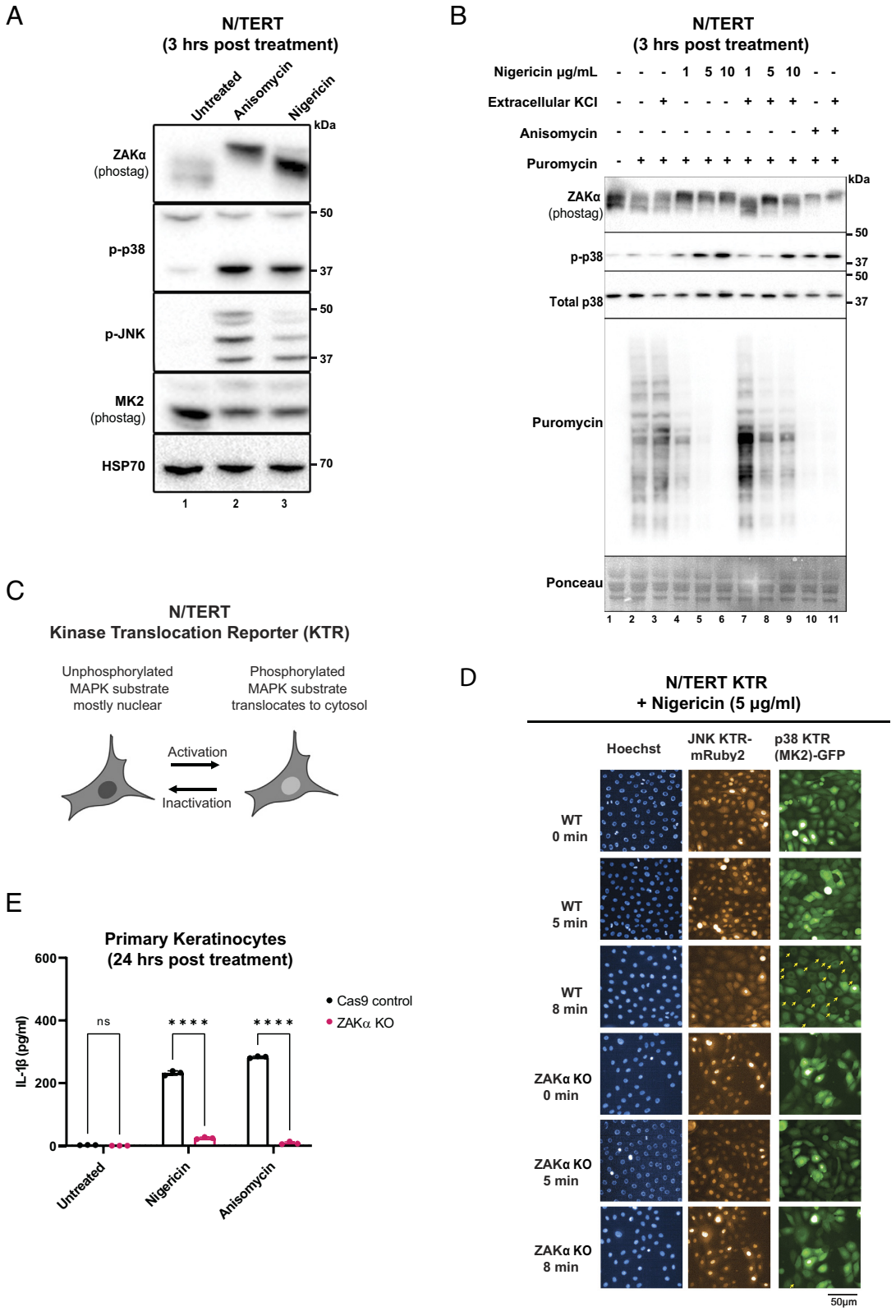

Fig. 4. (*A*) Immunoblotting of ZAKα and MK2 (PhosTag SDS-PAGE) and p-p38, p-JNK, and HSP70 (SDS-PAGE) in N/TERTs pretreated with emricasan (5 μM) and stimulated with nigericin (5 μg/mL) or anisomycin (1 μM) for 3 h. (*B*) ZAKα (PhosTag SDS-PAGE) and p-p38, total p38, and puromycin (SDS-PAGE) in N/TERTs pretreated with emricasan (5 μM) and stimulated with nigericin (5 μg/mL) or anisomycin (1 μM) ± extracellular KCl (50 mM) for 3 h. Ponceau staining was used as the loading control. Immunoblot shows lysates from one experiment performed three independent times. (*C*) Schematic of the phosphorylation-mediated kinase translocation reporter (KTR) system. (*D*) WT or ZAKα KO N/TERTs stably expressing JNK KTR-mRuby2 and MK2-mEGFP were pretreated with emricasan (5 μM) and stimulated with nigericin (5 μg/mL). Representative fluorescence images at 5 min and 8 min posttreatment at 20× magnification are shown. Images are shown from one experiment and are representative of n = 3 independent experiments; scale bar, 50 μm. Yellow arrows indicate cells with cytoplasmic translocation of the KTR signals. (*E*) ELISA showing IL-1β secretion in Cas9 control or ZAKα KO primary keratinocytes after nigericin (5 μg/mL) or anisomycin (1 μM) treatment. Supernatant was harvested 24 h posttreatment. Error bars represent SEM from three biological replicates, where one replicate refers to independent seeding and treatment of cells. Significance values were calculated based on two-way ANOVA followed by Sidak's test for multiple pairwise comparisons (*E*). ns, nonsignificant; ****$P < 0.0001$.

Table 1. Properties of molecules tested and their effects on RSR and NLRP1 inflammasome

		From literature				This study	
		Mechanism of ion transport	K+ selectivity*	Net charge	NLRP3 activation	ZAKα, p38, and JNK activation	Effect on human keratinocytes
Category I	Nigericin	Carrier ionophore: K+/H+ antiporter	Yes	Electroneutral	Yes	Yes	NLRP1-driven pyroptosis
	Lasalocid	Carrier ionophore: K+/H+ antiporter	Yes	Electroneutral	Yes (8)	Yes	NLRP1-driven pyroptosis
Category II	Valinomycin	Carrier ionophore: K+ uniporter	Yes	Electrogenic	Yes (41)	No	–
	Salinomycin	Carrier ionophore: Na+/H+ antiporter	No	Electroneutral	Unknown	No	–
	Monensin	Carrier ionophore: Na+/H+ antiporter	No	Electroneutral	No (42)	No	–
	Nonactin	Carrier ionophore: K+/NH4+ uniporter	Yes	Electrogenic	Unknown	No	–
	BME-44	Carrier type ionophore, K+ uniporter	Yes	Electrogenic	Yes (11)	No	–
Category III	Gramicidin	Channel formation; permeable to both K+ and Na+	No	Electroneutral	Yes (9)	Yes	Caspase-independent lytic cell death
	Palytoxin	Locks Na+/K+ pumps in the open state, creating open channels for Na+ and K+ and other cations	No	Electroneutral	Unknown	Yes	Caspase-independent lytic cell death

*Refers to cations such as K+ and Na+. Excluding protons.

dissipation of the membrane potential. We confirmed that gramicidin at 1 μM caused rapid K+ efflux to a similar extent as 6.7 μM nigericin (*SI Appendix*, Fig. S15*D*). In support of our hypothesis linking K+ efflux and RSR, gramicidin and palytoxin both induced rapid loss of puromycin incorporation and abolished ribosome runoff (Fig. 5*F*). This is accompanied by SAPK phosphorylation and ZAKα autophosphorylation (Fig. 5*A*). ZAKα KO partially but significantly reduced p38 and JNK phosphorylation induced by gramicidin and palytoxin (*SI Appendix*, Fig. S12*B*), suggesting that other stress-responsive MAPK pathways are also activated. Supplementation of extracellular potassium in palytoxin-treated cells rescued global protein translation and dampened p38 and JNK phosphorylation (*SI Appendix*, Fig. S12*D*). However, in contrast to nigericin and lasalocid, neither gramicidin nor palytoxin activates the NLRP1 inflammasome (Fig. 5*B*) or the hyperphosphorylation of the NLRP1 linker domain that is characteristic of ZAKα-driven NLRP1 activation (*SI Appendix*, Fig. S12*C*). We thus hypothesized that other pathways inhibit NLRP1-driven pyroptosis in palytoxin- and gramicidin-treated cells downstream of RSR. By tracking the fate of cells via live imaging, we found that both palytoxin and gramicidin cause rapid membrane swelling, but these "ballooned" cells, unlike pyroptotic cells, only take up PI with a significant delay (>30 min) (*SI Appendix*, Fig. S15*A*). This is in sharp contrast to ANS- and Nigericin-treated cells, where PI inclusion invariably occurs within 5 min or sometimes precedes visible membrane ballooning. Crucially, gramicidin- and palytoxin-induced lysis cannot be inhibited by the pan-caspase inhibitor, emricasan (*SI Appendix*, Fig. S15 *B* and *C*). These observations suggest that palytoxin and gramicidin do not cause pyroptosis, but instead kill the cells via direct osmotic lysis, likely mediated by water influx. This notion is fully supported by the physical dimensions of these channels. Gramicidin channels are ~4Å in diameter (48), whereas palytoxin locks the Na+/K+ ATPase pump into an open channel with an inner diameter of ~7Å (46). Thus, both channels are large enough to allow free passage of monovalent cations as well as water molecules (~2Å) (*SI Appendix*, Fig. S15*E*). The channel/pore dimensions also explain why gramicidin- and palytoxin-lysed cells do not become immediately permeable to PI as seen in nigericin- or lasalocid-treated cells: Propidium ions are ~15Å in diameter and are too large to pass through the palytoxin- and gramicidin-induced channels (49) but can easily pass through GSDMD pores, which are >200Å in diameter. We further postulate that rapid osmotic lysis interferes with NLRP1 phosphorylation and inflammasome activation at the level of NLRP1 linker phosphorylation (*SI Appendix*, Fig. S12*C*), although additional experiments are required to confirm this notion and decipher the biochemical details.

In summary, these results demonstrate that NLRP1 and NLRP3 have differing sensitivities toward membrane-disrupting agents. While NLRP3 can be activated by multiple triggers that cause K+ efflux, ZAKα-driven RSR and the NLRP1 inflammasome activation likely requires a higher threshold of K+ efflux. Thus, only electroneural, K+ selective ionophores such as nigericin and lasalocid acid activate NLRP1 in a ZAKα-dependent manner in primary human epithelial cells. Electrogenic K+ ionophores such as valinomycin do not activate RSR or NLRP1 efficiently in primary human keratinocytes, despite their known ability to activate NLRP3 in hematopoietic cells. Channel-forming molecules such as palytoxin and gramicidin, which cause electroneutral membrane permeabilization via simultaneous K+ efflux and Na+ influx, also activate ZAKα-driven RSR, but the concomitant osmolytic lysis likely interferes with NLRP1 activation.

Discussion

In this study, we demonstrate that cytosolic K+ efflux elicited by ionophores such as nigericin and lasalocid is a common trigger for two different inflammasome sensors: NLRP1 in primary human epithelial cells and NLRP3 in hematopoietic cells. In multiple types

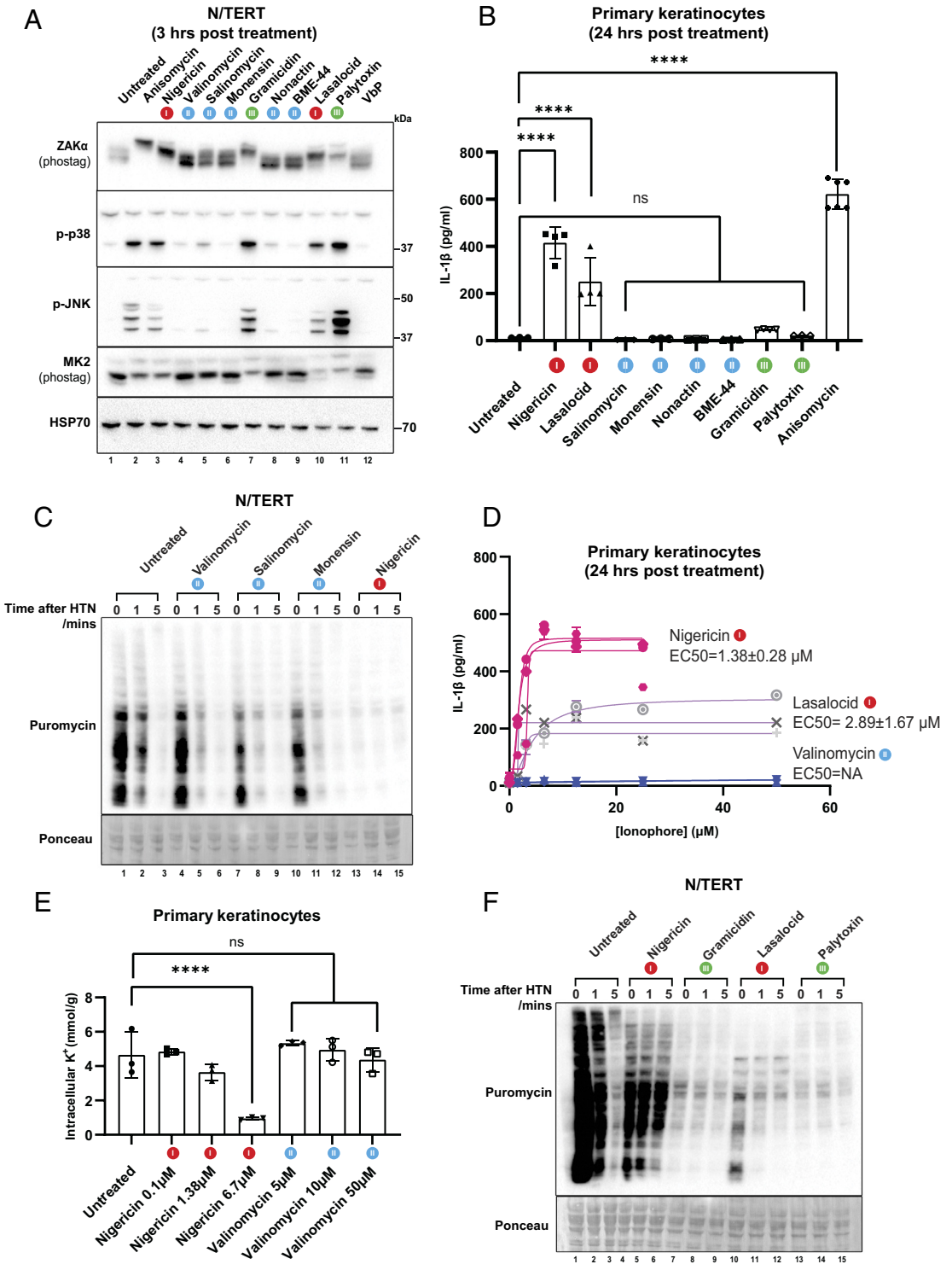

Fig. 5. (*A*) Immunoblotting of ZAKα and MK2 (PhosTag SDS-PAGE) or p-p38, p-JNK, and HSP70 (SDS-PAGE) in WT N/TERTs pretreated with emricasan (5 μM) and stimulated with anisomycin (1 μM), nigericin (5 μg/mL), valinomycin (5 μM), salinomycin (5 μM), monensin (5 μM), gramicidin (1 μM), nonactin (5 μM), BME-44 (5 μM), lasalocid (5 μM), palytoxin (100 pM), or VbP (3 μM) for 3 h. Immunoblot shows lysates from one experiment performed three independent times. (*B*) ELISA showing IL-1β secretion in supernatant of primary keratinocytes following treatment with nigericin (5 μg/mL), lasalocid (5 μM), salinomycin (5 μM), monensin (5 μM), nonactin (5 μM), BME-44 (5 μM), gramicidin (1 μM), palytoxin (100 pM), or anisomycin (1 μM). Supernatant was harvested 24 h posttreatment. (*C*) Immunoblotting of puromycin in WT N/TERTs pretreated with emricasan (5 μM) and stimulated with valinomycin (5 μM), salinomycin (5 μM), monensin (5 μM), or nigericin (5 μg/mL). Ponceau staining was used as the loading control. Immunoblot shows lysates from one experiment performed three independent times. (*D*) IL-1β ELISA showing half-maximal response (EC50) of nigericin, lasalocid and valinomycin in primary keratinocytes. Supernatant was harvested 24 h posttreatment (n = 3). Nigericin values are replotted from *SI Appendix*, Fig. S1*C* for ease of comparison. (*E*) Quantification of intracellular K^+ content by direct potentiometry in primary keratinocytes pretreated with emricasan (5 μM) and stimulated with nigericin (0.1 μM/1.38 μM/6.7 μM) or valinomycin (5 μM/10 μM/50 μM) for 5 min (n = 3). (*F*) Immunoblotting of puromycin in N/TERTs following a ribosome runoff assay. Cells were pretreated with emricasan (5 μM) and stimulated with nigericin (5 μg/mL), gramicidin (1 μM), lasalocid (5 μM), or palytoxin (100 pM) for 3 h before the addition of harringtonine (2 μg/mL) for the respective durations. Runoff was terminated by puromycin (10 μg/mL) for 10 min. Ponceau staining was used as the loading control. Immunoblot shows lysates from one experiment performed three independent times. Error bars represent SEM from three biological replicates, where one replicate refers to independent seeding and treatment of cells. Significance values were calculated based on one-way ANOVA followed by Dunnett's test (*B* and *E*). ns, nonsignificant; ****$P < 0.0001$.

of primary epithelial cells, nigericin causes rapid K+ efflux–dependent cessation of protein synthesis and ribosome stalling, which in turn activates ZAKα-driven RSR and SAPKs. The combined action of ZAKα and p38 kinase then drives NLRP1 activation through the hyperphosphorylation of its linker domain.

It is well known that human NLRP1 and NLRP3 have nonoverlapping cofactors, agonist repertoire as well as tissue distribution (12, 16–18, 23, 24, 50). While NLRP3 is mostly expressed in cells of hematopoietic origin, human NLRP1 is preferentially expressed in epithelial cells in the skin and airway. In fact, primary skin and airway epithelial cells, at least when cultured in vitro, do not express NLRP3 at all. Furthermore, NLRP1 and NLRP3 mutations cause distinct human diseases (51). Our results here, however, demonstrate that NLRP1 and NLRP3 could sense a common trigger: the loss of potassium ion homeostasis. That said, only a small subset of K+ ionophores, exemplified by nigericin and lasalocid acid are able to activate both NLRP1 and NLRP3. By comparing a panel of electrogeic and electroneutral ionophores in detail, we infer that ZAKα-driven NLRP1 activation requires a greater degree of K+ efflux than NLRP3. Thus, NLRP1 can only be achieved by K+ ionophores that cause a large amount of K+ efflux (category I in Table 1). Electrogenic K+ ionophores (e.g., valinomycin) which cause subtler changes in intracellular K+ levels are unable to activate RSR or NLRP1 (category II in Table 1). In additional support for this notion, earlier studies have shown that nigericin and lasalocid acid are also more efficient than valinomycin at activating NLRP3 (8).

We also showed that more drastic membrane perforation caused by gramicidin channels and palytoxin-hijacked Na+/K+ pumps (category III in Table 1) also activate ZAKα-driven RSR and SAPK activation, but fail to activate the NLRP1-driven pyroptosis. This is most likely due to interference from direct osmolysis caused by sodium and water influx at the level of NLRP1 phosphorylation. This finding shed light on the toxicology of these molecules. For instance, palytoxin exposure has been shown to cause respiratory distress as well as skin lesions (42). It is likely that rapid induction of ZAKα and osmotic lysis of epithelial cells both contribute to the pathogenesis of palytoxin poisoning.

In summary, we show here that K+ efflux is a broad-acting danger signal that activates RSR and commits multiple human cell types to pyroptotic cell death via distinct inflammasome sensors (*SI Appendix*, Fig. S15*F*). Considering that most of the known ionophores, including nigericin, are microbial metabolites, we speculate that the shared ability of NLRP1 and NLRP3 to sense K+ efflux allows them to collaboratively defend multiple organs against certain uncharacterized pathogen/pathogen(s). In this regard, it is interesting to note that regulated membrane depolarization has recently been found to play an active role in CRISPR-mediated antiphage immunity in bacteria (43). Our results also strengthen the recently described connection between ZAKα-dependent RSR and inflammation and give credence to the "HAMP" hypothesis (52), which posits that the human innate immune system monitors key homeostatic processes (e.g., ribosome elongation and membrane potential in this study) in order to respond to a wide variety of seemingly unrelated triggers using a limited number of sensor proteins.

Methods

Cell Culture and Chemicals. 293Ts (ATCC, #CRL-3216), A549-ASC-GFP-NLRP1 (InvivoGen, a549-ascg-nlrp1), THP-1 (Invivogen, thpd-nfis), U937 (ATCC, #CRL-1593.2*), U20S (ATCC, #HTB-96), and HeLa (ATCC, #CCL2) were cultured according to the manufacturer's protocol. Immortalized human keratinocytes (N/TERT) were provided by H. Rheinwald (MTA) and were cultured in Keratinocyte Serum Free Media (Gibco, 17005042), supplemented with 294.4 ng/L human recombinant Epidermal Growth Factor (EGF) (Gibco, 10450-013), 25 mg/L Bovine Pituitary Extract (Gibco, 13028-014), and 300 μM of $CaCl_2$ (Kanto Chemicals, 07058-00). Cell culture experiments involving immortalized cells or cell lines are conducted under Biological Project Number (BPN-72-2021) approved by the Institutional Biosafety Committee (NTU, Singapore). Primary human keratinocytes were derived from the foreskin of healthy donors and obtained with informed consent from the Asian Skin Biobank (ASB) (https://www.a-star.edu.sg/sris/technology-platforms/asian-skin-biobank). All primary keratinocyte experiments were carried out with approval from the A*STAR Human Biomedical Research Office (A*STAR Full IRB-2020-209). pHCEs (Sigma-Aldrich, SCCE016) were cultured according to the manufacturer's protocol. pHNECs were obtained and cultured as previously described (29). All cell lines used in this study underwent routine mycoplasma testing with MycoGuard (GeneCopoeia #LT07-118). The chemicals used in this study are listed in *SI Appendix, Materials and Methods*.

Cytokine Analysis. Human IL-1β enzyme-linked immunosorbent assay (ELISA) kit (BD, #557953) and human IL-18 ELISA kit (R&D, DY318-05) were used in accordance with the manufacturer's protocols to measure secreted cytokines.

Propidium Iodide Inclusion Assay. Primary keratinocytes of various genotypes were seeded in a black 12-well plate (Cellvis, P12-1.5P) at a density of 1.8×10^5 cells per well. The following day, cells were treated with the respective chemicals and stained with 0.5 μg/mL of propidium iodide (PI, Abcam #ab14083) before the plate was loaded into a high-content screening microscope (Perkin Elmer Operetta CLS imaging system, NTU Optical Bio-Imaging Centre in Nanyang Technological University, Singapore) for overnight imaging. Brightfield and fluorescence (PI channel, 536 nm/617 nm) were captured every 15 min. Images were then stored and analyzed using the Harmony software (Version 6). Using data acquired from five fields of view per well with three wells per treatment, the ratio of PI-positive cells over the total number of cells was calculated. The number of live cells per field was calculated using digital phase contrast images which allows for the identification of cell borders. The number of PI-positive stained cells was identified through the PI channel and counted as PI-positive cells.

Harringtonine Ribosome Runoff Assay. N/TERT cells were seeded at a cell density of 80,000 cells/well in a 24-well plate. The next day, cells were pretreated with 5 μM of emricasan for 30 min followed by treatment with the relevant ionophores or anisomycin for 3 h. The respective samples were treated with 2 μg/mL of harringtonine at staggered time points of 5, 1, and 0 min (equivalent to mock untreated). Cells were then pulsed with a final concentration of 10 μg/mL puromycin at the same time in all wells for 10 min. Following puromycin treatment, the supernatant was discarded and cells were lysed directly in 1× Laemmli buffer. Immunoblotting of samples using an anti-puromycin antibody was done to measure the amount of nascent peptides with puromycin incorporated, which reflects the rate of elongation after treatment.

CRISPR-Cas9 Knockout. MAP3K20 (ZAKα) KO N/TERT keratinocytes were made and described in detail previously (29). MAP3K20 (ZAKα) KO human primary keratinocytes were generated using lentiviral Cas9 and guide RNA plasmid (LentiCRISPR-V2, Addgene plasmid #52961) using the following guides: sg1 (TGTATGGTTATGGAACCGAG), sg4 (TGCATGGACGGAAGACGATG). NLRP1 KO human primary keratinocytes were generated using lentiviral transduction with the following guide: sg1 (GATAGCCCGAGTGCATCGG). A549-ASC-GFP-NLRP1 MAP3K20 (ZAKα) KO cells were generated using transfection of pSpCas9 plasmids with sgRNA into cells, followed by a diphtheria toxin selection method. In brief, A549 cells were seeded with a density of 100,000 cells in a 12WP. Cells were transfected using FuGENE HD on the next day with two separate pSpCas9-2A-puro plasmids, one encoding MAP3K20 guide 4(TGCATGGACGGAAGACGATG) and another encoding HBEGF guide 10 (CACCTCTCTCCATGGTAACC), in a 4:1 ratio. 2 d posttransfection, cells were treated with 20 ng/mL of diphtheria toxin(DT) for selection. Only cells that have the DT entry receptor HBEGF knocked out would survive DT treatment and would likely have undergone gene editing in the MAP3K20 gene. Knockout efficiency was tested by immunoblot. Alternatively, Sanger sequencing of genomic DNA and overall editing efficiency were determined using the Synthego ICE tool (Synthego Performance Analysis, ICE Analysis. 2019. v2.0. Synthego, https://ice.synthego.com/#/). The generation of NLRP1 KO pHECs and NLRP1 KO pHCEs have been described previously (31).

Inflammasome Activation. THP-1 monocytes were seeded at a density of 5×10^5 cells per well in a 12-well plate and were differentiated with 200 ng/mL PMA in R10 media (RPMI + 10% FBS) overnight and subsequently primed with 1 μg/mL LPS for 3 h. LPS-primed cells were then treated with 5uM MCC950 for 30 minutes and stimulated with nigericin (5 ug/mL). The following day, cell-free supernatant was harvested for IL-1β detection by ELISA, and western blot analysis was performed on the cell lysates. U937 monocytes were seeded at a density of 5×10^5 cells per well in a 12-well plate and were differentiated with 200 ng/mL PMA in R10 media (RPMI + 10% FBS) for 48 h. Forty-eight hours postdifferentiation, U937 macrophages were primed with 100 ng/mL LPS for 3 h. The medium was then replaced with serum-free RPMI 1640 medium and pretreatment with 5 μM MCC950 followed by overnight treatment with 5 μg/mL nigericin, 1 μM gramicidin or 5 μM Salinomycin was performed. The following day, cell-free supernatant was harvested for IL-1β detection by ELISA. Human primary keratinocytes were seeded at a density of 1.8×10^5 cells in a 12-well plate the day before stimulation. The following day, overnight stimulation was performed. Cell-free supernatant was harvested for IL-1β detection by ELISA, and western blot analysis was performed on the cell lysates. For detection of ASC specks and caspase-1 activation by immunofluorescence staining, treatment with 5 μg/mL nigericin and 1 μM anisomycin was performed for 3 h in the presence of 5 μM emricasan. pHNECs and pHCEs were seeded at a density of 2×10^5 cells per well in a 12-well plate the day before stimulation. The following day, medium was replaced with OPTIMEM, and cells were treated with 5 μM nigericin overnight. The following day, cell-free supernatant was harvested for IL-18 detection by ELISA. Treatment for 3 h with 10 μg/mL Nigericin and 1 μM anisomycin was performed in A549-ASC-GFP-NLRP1 cells for the detection of ASC specks. N/TERTs were seeded at a density of 0.8×10^5 cells in a 12-well plate. The following day, cells were primed overnight with TNFα. Subsequently, overnight stimulation with 5 μg/mL nigericin, 1 μM anisomycin, or 3 μM VbP was performed. The following day, cell-free supernatant was harvested for IL-1β detection by ELISA.

Polysome Profiling. Cells were exposed to nigericin (10 μg/mL) for the indicated times. Following treatment, cytosolic lysates were prepared using 20 mM Hepes pH 7.5, 100 mM NaCl, 5 mM $MgCl_2$, 100 mg/mL digitonin, 100 mg/mL cycloheximide, 1X protease inhibitor cocktail (Sigma, #P2714), and 200 U RiboLock RNase Inhibitor (Thermo Fisher Scientific, #EO0382). Extracts were pushed 10 times through a 26-G needle and incubated on ice for 5 min prior to centrifugation at 17,000 g for 5 min at 4 °C. After adding calcium chloride to a final concentration of 1 mM, lysates were optionally digested with 500 U micrococcal nuclease (MNase) (New England Biolabs, #M0247) for 30 min at 22 °C. Digestion was terminated by adding 2 mM EGTA. Equivalent amounts of lysate (150 mg of undigested RNA or 180 mg of MNase-digested RNA) were resolved in 15 to 50% sucrose gradients by centrifugation at 38,000 rpm in a Sorvall TH64.1 rotor for 2.5 h at 4 °C. The gradients were analyzed using a Biocomp density gradient fractionation system with continuous monitoring of the absorbance at 260 nm.

Measurement of Intracellular K+ Using Potentiometry and Flame Photometry. Human primary keratinocytes or N/TERTs were seeded at a cell density of 1.8×10^5 cells per well in a 12-well plate. The next day, cells were pretreated with 5 μM emricasan followed by treatment with the relevant ionophores for 5 min. Upon treatment, the supernatant was discarded, and cells were briefly washed twice with a K+ free buffer–TBS pH 7.5 (50 mM Tris-Cl+ 150 mM NaCl). Cells were then lysed in deionized water and subjected to two rounds of freeze-thaw cycles and stored at −80 °C. On the day of K+ quantification, lysates were centrifuged at 16,000 g for 10 min at 4 °C, and the supernatant was harvested for K+ concentration quantification by direct potentiometry (Siemens ADVIA 1800 analyzer) as well as total cellular protein concentration measurement. Normalized intracellular K+ content is calculated by dividing the K+ concentration of the lysate with the total protein concentration, with a final unit of mmol/g.

To determine intracellular K+ concentrations in A549 cells stably expressing NLRP1, cells were seeded at a cell density of 1×10^6 cells per well in a six-well plate. The next day, cells were treated with the relevant ionophores. At the time of harvesting, cell culture supernatant was discarded, and cells were washed twice with deionized water and then lysed in 1 mL of 10% nitric acid. Intracellular K+ content was measured by flame photometry (ICAP 6300 Thermo Generator RF). Absolute quantitation was obtained using standard solutions of potassium chloride.

Statistical Analysis. Statistical analyses were performed using Prism 9 (GraphPad Software, Inc.). Otherwise written, data are reported as mean with SEM. The methods for statistical analysis were included in the figure legend.

Data, Materials, and Software Availability. All study data are included in the article and/or *SI Appendix*.

ACKNOWLEDGMENTS. We are grateful for useful discussion and scientific advice from all members of the Zhong lab. We would like to thank Dr. Esther Koh (NOBIC) for assistance with image acquisition and analysis. We also thank Dr. Tomasz Próchnicki and Prof. Eicke Latz (University of Bonn, Germany) for sharing their experience and knowledge on NLRP3. Illustrations used in this manuscript were created with https://www.BioRender.com. Work from F.Z.'s lab is funded by the National Research Foundation Fellowship, Singapore (NRF-NRFF11-2019-0006), and Nanyang Assistant Professorship (NAP). Work from J.C.C.'s group is supported by the Singapore Ministry of Health's National Medical Research Council under its Open Fund Large Collaborative Grant (MOH-000271). Work in the S.B.-J.'lab is supported by the European Research Council (ERC) under the European Union's Horizon 2020 research and innovation program (grant agreement 863911–PHYRIST). Work from E.M.'s group is supported by the European Research Council (ERC) (ERC Starting Grant INFLAME 804249) and the French National Agency for Research (ANR, PSICOPAK).

Author affiliations: [a]Lee Kong Chian School of Medicine, Nanyang Technological University, 308232, Singapore; [b]Institute of Pharmacology and Structural Biology, University of Toulouse, CNRS, Toulouse 31077, France; [c]Center for Healthy Aging, University of Copenhagen, Copenhagen 2200, Denmark; [d]Center for Gene Expression, Department of Cellular and Molecular Medicine, University of Copenhagen, Copenhagen 2200, Denmark; [e]Agency for Science, Technology and Research (A*STAR) Skin Research Labs, 138648, Singapore; [f]Skin Research Institute of Singapore, 308232, Singapore; [g]Population and Global Health Program, Lee Kong Chian School of Medicine, Nanyang Technological University, 308232, Singapore; and [h]Department of Biological Sciences, National University of Singapore, 117543, Singapore

Author contributions: P.R., M.P., L.G., A.C.V., K.S.R., G.A.T., S.B.-J., E.M., and F.Z. designed research; P.R., M.P., L.G., A.C.V., K.S.R., G.A.T., M.J.F., J.F.M., S.K.K., Z.L., S.B.-J., E.M., and F.Z. performed research; J.C.C., E.M., and F.Z. contributed new reagents/analytic tools; P.R., M.P., L.G., A.C.V., K.S.R., G.A.T., M.J.F., J.F.M., S.K.K., Z.L., S.B.-J., E.M., and F.Z. analyzed data; and P.R., E.M., and F.Z. wrote the paper.

1. C. Howarth, P. Gleeson, D. Attwell, Updated energy budgets for neural computation in the neocortex and cerebellum. *J. Cereb. Blood Flow Metab.* **32**, 1222–1232 (2012).
2. D. Enkvetchakul, Genetic disorders of ion channels. *Mo. Med.* **107**, 270–275 (2010).
3. E. C. Cooper, L. Y. Jan, Ion channel genes and human neurological disease: Recent progress, prospects, and challenges. *Proc. Natl. Acad. Sci. U.S.A.* **96**, 4759–4766 (1999).
4. V. Kaushik, J. S. Yakisich, A. Kumar, N. Azad, A. K. V. Iyer, Ionophores: Potential use as anticancer drugs and chemosensitizers. *Cancers* **10**, 360 (2018).
5. A. Wong, Unknown risk on the farm: Does agricultural use of ionophores contribute to the burden of antimicrobial resistance? *mSphere* **4**, e00433-19 (2019).
6. D. G. Nicholls, S. J. Ferguson, "Ion transport across energy-conserving membranes" in Bioenergetics, D. G. Nicholls, S. J. Ferguson, Eds. (Academic Press, Cambridge, MA, ed. 4, 2013), pp. 13–25.
7. Y. He, H. Hara, G. Núñez, Mechanism and regulation of NLRP3 inflammasome activation. *Trends Biochem. Sci.* **41**, 1012–1021 (2016).
8. D. Perregaux, C. A. Gabel, Interleukin-1 beta maturation and release in response to ATP and nigericin. Evidence that potassium depletion mediated by these agents is a necessary and common feature of their activity. *J. Biol. Chem.* **269**, 15195–15203 (1994).
9. R. Muñoz-Planillo *et al.*, K^+ efflux is the common trigger of NLRP3 inflammasome activation by bacterial toxins and particulate matter. *Immunity* **38**, 1142–1153 (2013).
10. V. Pétrilli *et al.*, Activation of the NALP3 inflammasome is triggered by low intracellular potassium concentration. *Cell Death Differ.* **14**, 1583–1589 (2007).
11. A. Tapia-Abellán *et al.*, Sensing low intracellular potassium by NLRP3 results in a stable open structure that promotes inflammasome activation. *Sci. Adv.* **7**, eabf4468 (2021).
12. M. M. Gaidt, V. Hornung, The NLRP3 inflammasome renders cell death pro-inflammatory. *J. Mol. Biol.* **430**, 133–141 (2018).
13. L. Xiao, V. G. Magupalli, H. Wu, Cryo-EM structures of the active NLRP3 inflammasome disc. *Nature* **613**, 595–600 (2023).
14. L. Andreeva *et al.*, NLRP3 cages revealed by full-length mouse NLRP3 structure control pathway activation. *Cell* **184**, 6299–6312.e22 (2021).
15. I. V. Hochheiser, M. Pilsl, G. Hagelueken, J. Moecking, Structure of the NLRP3 decamer bound to the cytokine release inhibitor CRID3. *Nature* **604**, 184–189 (2022).
16. Z. Zhang *et al.*, Distinct changes in endosomal composition promote NLRP3 inflammasome activation. *Nat. Immunol.* **24**, 30–41 (2023).

17. J. Chen, Z. J. Chen, PtdIns4P on dispersed trans-Golgi network mediates NLRP3 inflammasome activation. *Nature* **564**, 71–76 (2018).
18. B. Lee *et al.*, Disruptions in endocytic traffic contribute to the activation of the NLRP3 inflammasome. *Sci. Signal.* **16**, eabm7134 (2023).
19. L. Franchi, T.-D. Kanneganti, G. R. Dubyak, G. Núñez, Differential requirement of P2X7 receptor and intracellular K+ for caspase-1 activation induced by intracellular and extracellular bacteria. *J. Biol. Chem.* **282**, 18810–18818 (2007).
20. F. Liu *et al.*, Nigericin exerts anticancer effects on human colorectal cancer cells by inhibiting Wnt/β-catenin signaling pathway. *Mol. Cancer Ther.* **17**, 952–965 (2018).
21. G. Fenini *et al.*, Genome editing of human primary keratinocytes by CRISPR/Cas9 reveals an essential role of the NLRP1 inflammasome in UVB sensing. *J. Invest. Dermatol.* **138**, 2644–2652 (2018).
22. G. Fenini *et al.*, The p38 mitogen-activated protein kinase critically regulates human keratinocyte inflammasome activation. *J. Invest. Dermatol.* **138**, 1380–1390 (2018).
23. P. S. Mitchell, A. Sandstrom, R. E. Vance, The NLRP1 inflammasome: New mechanistic insights and unresolved mysteries. *Curr. Opin. Immunol.* **60**, 37–45 (2019).
24. C. Y. Taabazuing, A. R. Griswold, D. A. Bachovchin, The NLRP1 and CARD8 inflammasomes. *Immunol. Rev.* **297**, 13–25 (2020).
25. R. P. Lana, J. B. Russell, Use of potassium depletion to assess adaptation of ruminal bacteria to ionophores. *Appl. Environ. Microbiol.* **62**, 4499–4503 (1996).
26. K. S. Robinson *et al.*, Diphtheria toxin activates ribotoxic stress and NLRP1 inflammasome-driven pyroptosis. *J. Exp. Med.* **220**, e20230105 (2023).
27. J. Sand *et al.*, The NLRP1 inflammasome pathway is silenced in cutaneous squamous cell carcinoma. *J. Invest. Dermatol.* **139**, 1788–1797.e6 (2019).
28. M. A. Dickson *et al.*, Human keratinocytes that express hTERT and also bypass a p16(INK4a)-enforced mechanism that limits life span become immortal yet retain normal growth and differentiation characteristics. *Mol. Cell. Biol.* **20**, 1436–1447 (2000).
29. K. S. Robinson *et al.*, ZAKα-driven ribotoxic stress response activates the human NLRP1 inflammasome. *Science* **377**, 328–335 (2022).
30. L. Jenster *et al.*, P38 kinases mediate NLRP1 inflammasome activation after ribotoxic stress response and virus infection. *J. Exp. Med.* **220**, e20220837 (2022).
31. M. Pinilla *et al.*, EEF2-inactivating toxins engage the NLRP1 inflammasome and promote epithelial barrier disruption. *J. Exp. Med.* **220**, e20230104 (2023).
32. M. L. Vyleta, J. Wong, B. E. Magun, Suppression of ribosomal function triggers innate immune signaling through activation of the NLRP3 inflammasome. *PLoS One* **7**, e36044 (2012).
33. F. Cahn, M. Lubin, Inhibition of elongation steps of protein synthesis at reduced potassium concentrations in reticulocytes and reticulocyte lysate. *J. Biol. Chem.* **253**, 7798–7803 (1978).
34. A. Rozov *et al.*, Importance of potassium ions for ribosome structure and function revealed by long-wavelength X-ray diffraction. *Nat. Commun.* **10**, 2519 (2019).
35. R. J. Argüello *et al.*, SunRiSE – measuring translation elongation at single-cell resolution by means of flow cytometry. *J. Cell Sci.* **131**, jcs214346 (2018).
36. A. C. Vind *et al.*, ZAKα recognizes stalled ribosomes through partially redundant sensor domains. *Mol. Cell* **78**, 700–713.e7 (2020).
37. C.C.-C. Wu, A. Peterson, B. Zinshteyn, S. Regot, R. Green, Ribosome collisions trigger general stress responses to regulate cell fate. *Cell* **182**, 404–416.e14 (2020).
38. A. C. Vind, A. V. Genzor, S. Bekker-Jensen, Ribosomal stress-surveillance: Three pathways is a magic number. *Nucleic Acids Res.* **48**, 10648–10661 (2020).
39. D. M. Jandhyala, A. Ahluwalia, T. Obrig, C. M. Thorpe, ZAK: A MAP3Kinase that transduces Shiga toxin- and ricin-induced proinflammatory cytokine expression. *Cell. Microbiol.* **10**, 1468–1477 (2008).
40. H. Miura, Y. Kondo, M. Matsuda, K. Aoki, Cell-to-cell heterogeneity in p38-mediated cross-inhibition of JNK causes stochastic cell death. *Cell Rep.* **24**, 2658–2668 (2018).
41. S. Regot, J. J. Hughey, B. T. Bajar, S. Carrasco, M. W. Covert, High-sensitivity measurements of multiple kinase activities in live single cells. *Cell* **157**, 1724–1734 (2014).
42. M. Pelin, V. Brovedani, S. Sosa, A. Tubaro, Palytoxin-containing aquarium soft corals as an emerging sanitary problem. *Mar. Drugs* **14**, 33 (2016).
43. A. R. VanderWal *et al.*, Csx28 is a membrane pore that enhances CRISPR-Cas13b-dependent antiphage defense. *Science* **380**, 410–415 (2023).
44. L. Gurcel, L. Abrami, S. Girardin, J. Tschopp, F. G. van der Goot, Caspase-1 activation of lipid metabolic pathways in response to bacterial pore-forming toxins promotes cell survival. *Cell* **126**, 1135–1145 (2006).
45. R. Elber, D. P. Chen, D. Rojewska, R. Eisenberg, Sodium in gramicidin: An example of a permion. *Biophys. J.* **68**, 906–924 (1995).
46. P. Artigas, D. C. Gadsby, Large diameter of palytoxin-induced Na/K pump channels and modulation of palytoxin interaction by Na/K pump ligands. *J. Gen. Physiol.* **123**, 357–376 (2004).
47. P. Artigas, D. C. Gadsby, Na+/K+-pump ligands modulate gating of palytoxin-induced ion channels. *Proc. Natl. Acad. Sci. U.S.A.* **100**, 501–505 (2003).
48. A. Finkelstein, O. S. Andersen, The gramicidin A channel: A review of its permeability characteristics with special reference to the single-file aspect of transport. *J. Membr. Biol.* **59**, 155–171 (1981).
49. A. M. Bowman, O. M. Nesin, O. N. Pakhomova, A. G. Pakhomov, Analysis of plasma membrane integrity by fluorescent detection of Tl(+) uptake. *J. Membr. Biol.* **236**, 15–26 (2010).
50. N. A. Schmacke *et al.*, IKKβ primes inflammasome formation by recruiting NLRP3 to the trans-Golgi network. *Immunity* **55**, 2271–2284.e7 (2022).
51. S. Alehashemi, R. Goldbach-Mansky, Human autoinflammatory diseases mediated by NLRP3-, Pyrin-, NLRP1-, and NLRC4-inflammasome dysregulation updates on diagnosis, treatment, and the respective roles of IL-1 and IL-18. *Front. Immunol.* **11**, 1840 (2020).
52. A. Liston, S. L. Masters, Homeostasis-altering molecular processes as mechanisms of inflammasome activation. *Nat. Rev. Immunol.* **17**, 208–214 (2017).